Earthquakes and Structures, *Vol. 7, No. 2 (2014) 159-178*
DOI: http://dx.doi.org/10.12989/eas.2014.7.2.159

Numerical dissipation for explicit, unconditionally stable time integration methods

Shuenn-Yih-Chang *

Department of Civil Engineering, National Taipei University of Technology, NTUT Box 2653, Taipei 106, Taiwan, Republic of China

(Received December 29, 2013, Revised March 10, 2014, Accepted March 24, 2014)

Abstract. Although the family methods with unconditional stability and numerical dissipation have been developed for structural dynamics they all are implicit methods and thus an iterative procedure is generally involved for each time step. In this work, a new family method is proposed. It involves no nonlinear iterations in addition to unconditional stability and favorable numerical dissipation, which can be continuously controlled. In particular, it can have a zero damping ratio. The most important improvement of this family method is that it involves no nonlinear iterations for each time step and thus it can save many computationally efforts when compared to the currently available dissipative implicit integration methods.

Keywords: unconditional stability, numerical dissipation, nonlinear dynamic analysis, accuracy, structure-dependent integration method

1. Introduction

In general, the vibration problems governed by the equations of motion can be categorized into two types. One is inertial problems and the other is wave propagation problems. The class of inertial problems is also known as structural dynamics problems, to indicate that the response is dominated by low frequency modes only. The wave propagation problems are the shock response from impact and explosions and the problems where wave effects are important, to indicate that both low and high frequency modes contribute to the response. It is recognized that the inertial problems are best solved by implicit algorithms (Newmark 1959; Bathe and Wilson 1973; Krieg 1973; Dobbs 1974; Belytschko and Schoeberle 1975; Zienkiewicz 1977; Belytschko and Hughes 1983; Hughes 1987), while explicit algorithms (Newmark 1959) are more appropriate for wave propagation problems. This is because that an implicit algorithm can have unconditional stability, and thus a larger time step can be used since the high frequency modes are unimportant for inertial problems. On the other hand, the major advantage of explicit algorithms is the explicitness of each time step and thus the computation cost of a single time step is much cheaper than for an implicit method since it involves no nonlinear iterations. Hence, if high frequency responses are important, then the time steps required to accurately integrate these high frequency modes will satisfy the upper stability limit automatically.

*Corresponding author, Professor, E-mail: changsy@ntut.edu.tw.

http://www.techno-press.org/?journal=eas&subpage=7 ISSN: 2092-7614 (Print), 2092-7622 (Online)

Some structure-dependent integration methods (Chang 2002, 2007, 2009, 2010) have been proposed to integrate the major advantages of the implicit and explicit algorithms together, i.e., the unconditional stability of implicit algorithms and no nonlinear iterations of explicit algorithms. As a result, they are promising for solving inertial problems. However, these methods have no numerical dissipation although favorable numerical dissipation can be used to suppress any spurious growth of high frequency modes. Among the currently available integration methods, some family methods were developed to have favorable numerical dissipation, such as Wilson θ method (Bathe and Wilson, 1973), HHT $-\alpha$ method (Hilber *et al*. 1977), WBZ $-\alpha$ method (Wood *et al*. 1981), generalized $-\alpha$ method (Chung and Hulbert 1993) and the methods developed by Zhou and Tamma (2004, 2006). All these dissipative integration methods are implicit algorithms and thus an iterative procedure is generally needed. Therefore, it seems valuable if numerical dissipation can be further introduced into the previously developed structure-dependent integration methods since they already have unconditional stability and involve no nonlinear iterations. For this purpose, a new family of structure-dependent integration methods with desired numerical dissipation was proposed and is presented herein, where both numerical properties and computational efficiency are explored.

2. Proposed family method

Consider the equation of motion for a single degree of freedom system

$$m\ddot{u} + c\dot{u} + ku = f \tag{1}$$

where m, c, k and f are the mass, viscous damping coefficient, stiffness and external force, respectively; and u, $\dot{u}$ and $\ddot{u}$ are the displacement, velocity and acceleration, respectively. A family method is proposed for the step-by-step solution of Eq. (1) and it can be written as

$$\begin{aligned} & ma_{i+1} + c_0 v_{i+1} + \frac{2p}{p+1} k_{i+1} d_{i+1} - \frac{p-1}{p+1} k_i d_i = \frac{2p}{p+1} f_{i+1} - \frac{p-1}{p+1} f_i \\ & d_{i+1} = \beta_0 d_{i-1} + \beta_1 d_i + \beta_2 (\Delta t) v_i + \beta_3 (\Delta t)^2 a_i \\ & v_{i+1} = v_i + \frac{3p-1}{2(p+1)} (\Delta t) a_i - \frac{p-3}{2(p+1)} (\Delta t) a_{i+1} \end{aligned} \tag{2}$$

where d_i, v_i, a_i and f_i are the nodal displacement, velocity, acceleration and external force at the $i-th$ time step respectively, Δt is a step size and k_i is the stiffness at the end of the $i-th$ time step. The coefficients β_0 to β_3 are found to be

$$\begin{aligned} \beta_0 &= -\frac{1}{D}\left[\frac{p-1}{8}\left(\frac{2}{p+1}\right)^3 \Omega_0^2\right] & \beta_1 &= 1 + \frac{1}{D}\left[\frac{p-1}{8}\left(\frac{2}{p+1}\right)^3 \Omega_0^2\right] \\ \beta_2 &= \frac{1}{D}\left(1 - \frac{p-3}{p+1}\xi\Omega_0\right) & \beta_3 &= \frac{1}{D}\left\{\tfrac{1}{2} - \tfrac{1}{2}\left[\left(\frac{2}{p+1}\right)^2 + \frac{p-3}{p+1}\right]\xi\Omega_0\right\} \end{aligned} \tag{3}$$

where ξ is a viscous damping ratio; $\Omega_0 = \omega_0 (\Delta t)$ and $\omega_0 = \sqrt{k_0 / m}$ is the natural frequency of the system determined from the initial stiffness of k_0. In addition, p is the parameter to govern the numerical properties and D is defined as

$$D = 1 - \frac{p-3}{p+1}\xi\Omega_0 + \frac{p}{4}\left(\frac{2}{p+1}\right)^3 \Omega_0^2 \tag{4}$$

The development details of this method are similar to those of the previously published algorithms (Chang 2009, 2010) and thus will not be elaborated herein.

For computationally efficiency, it is important to express $\xi\Omega_0$ and Ω_0^2 in terms of the initial structural properties and step size for a structure-dependent integration method (Chang 2009, 2010). Thus, the relations of $c_0 = 2\xi\omega_0 m$ and $\Omega_0^2 = (\Delta t)^2 (k_0 / m)$ are found from the fundamental theory of structural dynamics. After substituting these relations into Eqs. (3) and (4), they become

$$\beta_0 = -\frac{1}{D}\left[\frac{p-1}{8}\left(\frac{2}{p+1}\right)^3 (\Delta t)^2 k_0\right] \qquad \beta_1 = 1 + \frac{1}{D}\left[\frac{p-1}{8}\left(\frac{2}{p+1}\right)^3 (\Delta t)^2 k_0\right]$$

$$\beta_2 = \frac{1}{D}\left[m - \frac{p-3}{2(p+1)}(\Delta t) c_0\right] \qquad \beta_3 = \frac{1}{D}\left\{\tfrac{1}{2} m - \tfrac{1}{4}\left[\left(\frac{2}{p+1}\right)^2 + \frac{p-3}{p+1}\right](\Delta t) c_0\right\} \tag{5}$$

$$D = m - \frac{p-3}{2(p+1)}(\Delta t) c_0 + \frac{p}{4}\left(\frac{2}{p+1}\right)^3 (\Delta t)^2 k_0$$

These coefficients remain invariant for a whole integration procedure since they are determined from the initial structural properties of c_0 and k_0 if a fixed time step is also employed.

It is important to note that the two difference equations of the proposed family method (PFM) are structure dependent since their coefficients are functions of the initial structural properties m and k_0. Hence, this method is entirely different from the methods developed by Zhou and Tamma (2004, 2006) although theirs methods can cover almost all the second order methods. It is found that all the coefficients of the difference equations for the Zhou and Tamma's methods are constant values. In addition, they are implicit methods. It is manifested from the second line of Eq. (2) that the displacement d_{i+1} can be explicitly determined from the previous two step data and thus it is explicit. This is exactly the same as that for the Newmark explicit method (NEM), where the equation of motion for the $(i+1)-th$ time step is not involved in determining the displacement d_{i+1}. As a result, they involve no nonlinear iterations for a nonlinear systems.

3. Recursive matrix form

For free vibration, the proposed family algorithm can be succinctly expressed in a recursive matrix form (Bathe and Wilson 1973; Hilber *et al*. 1977; Hughes 1987) of

$$\mathbf{X}_{i+1} = \mathbf{A}\mathbf{X}_i \tag{6}$$

where $\mathbf{X}_{i+1} = \left[d_{i+1},\ (\Delta t)v_{i+1},\ (\Delta t)^2 a_{i+1}\right]^{\mathrm{T}}$ is defined, and $\mathbf{A}$ is an amplification matrix. Hence, the characteristic equation of $\mathbf{A}$ can be obtained from $|\mathbf{A} - \lambda\mathbf{I}| = 0$ and is found to be

$$\lambda^3 - A_1\lambda^2 + A_2\lambda - A_3 = 0 \tag{7}$$

where λ is an eigenvalue of the matrix $\mathbf{A}$ and the coefficients A_1, A_2 and A_3 are found to be

$$\begin{aligned}
A_1 &= 2 - \frac{2\xi\Omega}{D} + \frac{1}{D}\left[\frac{p-1}{8}\left(\frac{2}{p+1}\right)^3 - \frac{4p}{(p+1)^2}\right]\Omega^2 \\
A_2 &= 1 - \frac{2\xi\Omega}{D} + \frac{1}{D}\left[\frac{p-1}{4}\left(\frac{2}{p+1}\right)^3 + \frac{2(p-1)^2}{(p+1)^2}\right]\Omega^2 \\
A_3 &= \frac{1}{D}\left[\frac{p-1}{8}\left(\frac{2}{p+1}\right)^3 + \left(\frac{p-1}{p+1}\right)^2\right]\Omega^2
\end{aligned} \tag{8}$$

where B is further defined as

$$B = 1 - \frac{p-3}{p+1}\xi\Omega \tag{9}$$

for brevity. It is worth noting that for a linear elastic system $\Omega_0 = \Omega$ is taken in the corresponding equations.

4. Convergence

The convergence of a computational method is implied by the consistency and the stability based on the Lax equivalence theorem (Lax and Richmyer 1956). The consistency is in terms of the qualitative measure such as the order of accuracy determined from the local truncation error. In general, an algorithm is said to be convergent if it is both consistent and stable.

4.1 Consistency and local truncation error

A local truncation error is defined as the error committed in each time step by replacing the differential equation with its corresponding difference equation (Belytschko and Hughes 1983; Bathe 1986; Hughes 1987). The approximating difference equation for PFM can be obtained from Eq. (6) after eliminating velocities and accelerations and is found to be

$$d_{i+1} - A_1 d_i + A_2 d_{i-1} - A_1 d_{i-2} = 0 \tag{10}$$

Consequently, after replacing Eq. (1) by Eq. (10), the local truncation error for PFM is:

$$E = \frac{1}{(\Delta t)^2}\left[u(t+\Delta t) - A_1 u(t) + A_2 u(t-\Delta t) - A_3 u(t-2\Delta t)\right] \tag{11}$$

In addition, if $u(t)$ is assumed to be continuously differentiable up to any required order, the terms of $u(t+\Delta t)$ $u(t-\Delta t)$ and $u(t-2\Delta t)$ can be expanded into finite Taylor series at t. As a result, after substituting A_1 A_2 and A_3 into the resultant of Eq. (11), the local truncation error for PFM is found to be

$$\begin{aligned} E = {} & \frac{2\xi}{BD}\left(\frac{p-1}{p+1}\right)\Omega\omega^2 u + \frac{4\xi^2}{BD}\left(\frac{p-1}{p+1}\right)\Omega\omega\dot{u} + \frac{1}{BD}\left[\frac{1}{12} - \frac{1}{4}\left(\frac{2}{p+1}\right)^2 + \left(\frac{p-1}{p+1}\right)^2 + \frac{1}{3}\xi^2\right]\Omega^2\omega^2 u \\ & + \frac{\xi}{BD}\left[2\left(\frac{p-1}{p+1}\right)^2 - \frac{1}{2}\left(\frac{2}{p+1}\right)^2 + \tfrac{2}{3}\xi^2\right]\Omega^2\omega\dot{u} + O\left[(\Delta t)^3\right] \end{aligned} \tag{12}$$

for a linear elastic system. This equation reveals that PFM has a minimum order of accuracy 1 and thus its consistency is verified for any values of p and ξ. In addition, an order of accuracy 2 can be generally achieved for either $p = 1$ or $\xi = 0$.

4.1 Stability

Stability analysis of PFM is very complicated since it has three non-zero eigenvalues due to $A_3 \neq 0$, as shown in Eq. (8). Alternatively, stability conditions for the cases of $\Omega \to 0$ and $\Omega \to \infty$ are cautiously examined and are applied to find out the restrictions of the parameters p and ξ to have unconditional stability. As a result, in the limiting case of $\Omega \to 0$, Eq. (7) reduces to

$$\lambda(\lambda - 1)^2 = 0 \tag{13}$$

It is apparent that $\lambda_{1,2} \to 1$ and $\lambda_3 \to 0$; and these eigenvalues are independent of the parameters p and ξ. On the other hand, in the limit $\Omega \to \infty$, it is found to be

$$\left(\lambda - \frac{p-1}{2p}\right)\left\{\lambda^2 - \left[2 - 4\left(\frac{p+1}{2}\right)\right]\lambda + \left[1 + 2(p-1)\left(\frac{p+1}{2}\right)\right]\right\} = 0 \tag{14}$$

for any viscous damping ratio. The roots of this equation are plotted in Fig. 1 as functions of p. It is apparent that PFM is stable in the limit $\Omega \to \infty$ if $1/3 \le p \le 1$ is satisfied since in this range the spectral radius is always less than or equal to 1. This figure shows that the decrease of p below 1/2 will increase the spectral radius. Thus, it is implied that the range of $1/2 \le p \le 1$ is of interest.

After considering the limiting cases of $\Omega \to 0$ and $\Omega \to \infty$, the stability properties of PFM with $1/2 \le p \le 1$ for a general value of Ω are further evaluated by the Routh-Hurwitz criterion

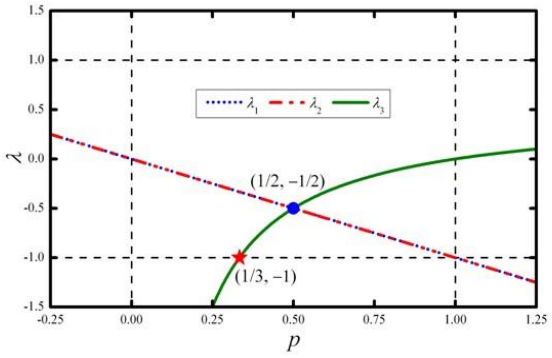

Fig. 1 Eigenvalues of amplification matrix as Ω tends to infinity

which gives necessary and sufficient conditions for the roots of polynomial to have negative real parts and following the procedure given by Lambert (1973). Hence, a necessary and sufficient condition for the roots of Eq. (7) to lie within or on the circle $|\lambda|=1$ is the satisfaction of the following inequalities:

$$\begin{aligned} &1-A_1+A_2-A_3\geq 0 \qquad && 3-A_1-A_2+3A_3\geq 0 \\ &3+A_1-A_2-3A_3\geq 0 \qquad && 1+A_1+A_2+A_3\geq 0 \\ &1-A_2+A_3\left(A_1-A_3\right)\geq 0 \end{aligned} \tag{15}$$

After substituting Eq. (8) into this equation, it is found that all the five inequalities will be met if $\xi\geq 0$ holds. This proves stability for PFM with the condition of $\xi\geq 0$. This fact of stability property in conjunction with the previous proof of consistency implies convergence for PFM.

5. Numerical properties for PFM

After the proof of the convergence of PFM, it is of great interest to further investigate its numerical properties for a linear elastic system. Since the evaluation techniques for an integration method can be easily found in the related references (Zienkiewicz 1977; Belytschko and Hughes 1983; Hughes 1987) and thus will not be elaborated here again.

5.1 Spectral radius

The variation of spectral radius with $\Delta t/T$ is shown in Fig. 2 for $p=1$, 0.75, 0.50 and 1/3. The spectral radius is always equal to 1 for $p=1$ and thus it is indicated that zero damping can be achieved for PFM. For each curve, the spectral radius is almost equal to 1 for a small value of $\Delta t/T$. Subsequently, it decreases gradually and finally tends to a certain value, which is smaller

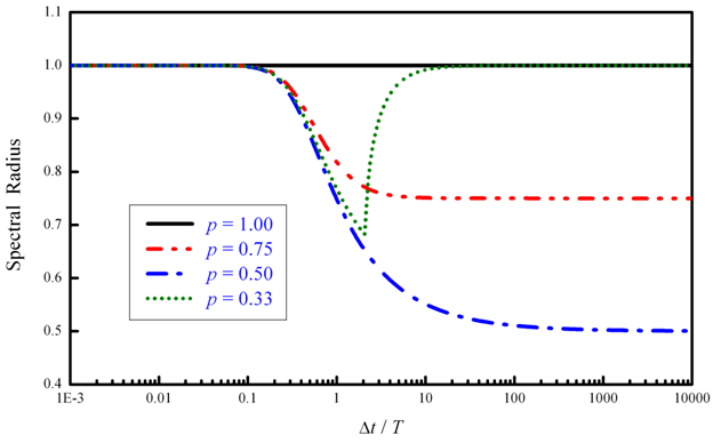

Fig. 2 Variation of spectral radius with $\Delta t / T$ for SPFM

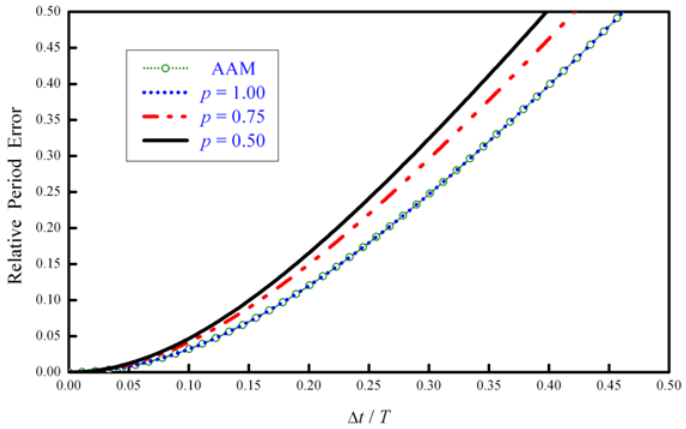

Fig. 3 Variation of relative period error with $\Delta t / T$ for different p values

than 1 for large $\Delta t / T$ for $p = 0.75$ and 0.50. It is also found this value generally decreases with the decrease of p until $p = 0.50$. This implies that PFM with $p = 0.50$ can provide the largest numerical dissipation for high frequency modes. It is clear that $p = 1/3$ cannot have the favorable dissipative property since the spectral radius approaches 1 for a large value of $\Delta t / T$.

5.2 Relative period error

Similarly, the variation of the relative period error with $\Delta t / T$ for PFM for various cases is shown in Fig. 3 while that for the numerical damping ratio is plotted in Fig. 4. In addition, those for the constant average acceleration method (AAM) are also plotted in the figures

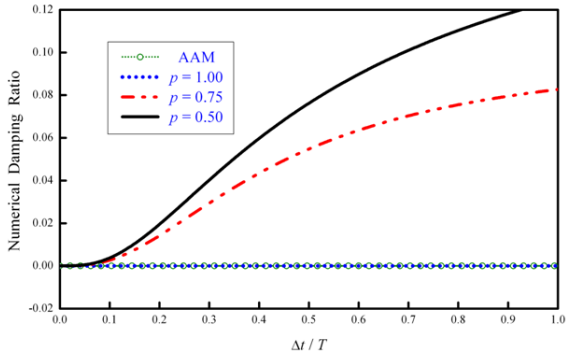

Fig. 4 Variation of numerical damping ratio with $\Delta t / T$ for different p values

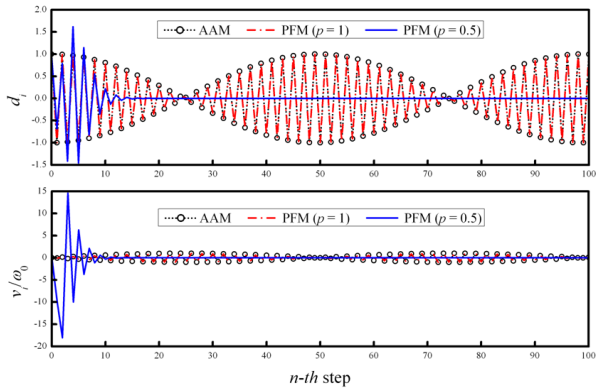

Fig. 5 Comparisons of overshoot responses

correspondingly for comparisons. Apparently, the relative period error increases with the decrease of p for a given value of $\Delta t / T$. In general, the relative period error is very small for a small value of $\Delta t / T$, say $\Delta t / T \le 0.05$, as $1/2 \le p \le 1$. Hence, its corresponding time step will lead to insignificant period distortion during the step-by-step integration. It is interesting to find that the curve for the case of $p = 1$ is almost coincided with that of AAM in Fig. 3. This implies that PFM with $p = 1$ will have exactly the same period distortion property as that of AAM.

5.3 Numerical damping

It is manifested from Fig. 4 that the continuous control of numerical damping is evident. In addition, the desired numerical damping properties are also achieved since there is a zero tangent at the origin and subsequently a controlled turn upward for the curves with $p = 0.75$ and 0.50. Hence, the higher modes can be suppressed or eliminated by numerical dissipation and at the same time the lower modes are almost unaffected. It is apparent that the case of $p = 1$ leads to no numerical dissipation and thus it has the least period distortion as shown in Fig. 3. Figs. 3 and 4

reveal that the increase of numerical dissipation for PFM will sacrifice its period distortion as it is found for a general dissipative integration method (Belytschko and Hughes 1983).

5.4 Overshooting

To evaluate the tendency of an integration method to overshoot the exact solutions (Goudreau and Taylor 1972; Hilber and Hughes 1978) one can compute the free vibration response of a single degree of freedom system for the current time step based on the previous step data. The behavior as $\Omega \to \infty$ gives an indication of the behavior of the high frequency modes. Using Eq. (6), the following equations can be obtained for the limiting condition of $\Omega \to \infty$.

$$d_{i+1} \approx \left[1 - \frac{(p+1)^3}{4p}\right] d_i \quad , \quad v_{i+1} \approx -(p-1)^2 \Omega \omega d_i + \left[\frac{(p-1)^2}{2} - 1\right] v_i \tag{16}$$

It is manifested from the first line of this equation that there is no overshoot in displacement for PFM while it has a tendency to overshoot linearly in Ω in the velocity equation due to the initial displacement term except for $p = 1$.

To confirm the overshoot behavior of PFM, the discrete displacement and velocity responses are obtained from PFM with $p = 1$ and 0.5. The free vibration to the initial conditions $d_0 = 1$ and $v_0 = 0$ is considered. A time step of $\Delta t = 10T$ is used. Numerical solutions are shown in Fig. 5. In addition, the results obtained from AAM are also plotted in the figure for comparison. The velocity term is normalized by the initial natural frequency of the system in order to have the same unit as displacement. Fig. 5 shows that the curves are overlapped together for AAM and PFM with $p = 1$ and exhibit no overshoot both in displacement and velocity. On the other hand, there is almost no overshooting in displacement for PFM with $p = 0.5$ while a significant overshoot in velocity is found. These numerical results are consistent with analytical results.

6. Implementation details

It is of great interest to apply PFM to perform some dynamic analyses to confirm its favorable numerical properties. Consequently, the implementation details of PFM for a multiple degree of freedom system are presented next. The general formulation for PFM can be written as

$$\begin{aligned}
&\mathbf{M}\mathbf{a}_{i+1} + \mathbf{C}_0 \mathbf{v}_{i+1} + \frac{2p}{p+1}\mathbf{K}\mathbf{d}_{i+1} - \frac{p-1}{p+1}\mathbf{K}\mathbf{d}_i = \frac{2p}{p+1}\mathbf{f}_{i+1} - \frac{p-1}{p+1}\mathbf{f}_i \\
&\mathbf{d}_{i+1} = \mathbf{B}_0 \mathbf{d}_{i-1} + \mathbf{B}_1 \mathbf{d}_i + \mathbf{B}_2 (\Delta t)\mathbf{v}_i + \mathbf{B}_3 (\Delta t)^2 \mathbf{a}_i \\
&\mathbf{v}_{i+1} = \mathbf{v}_i + \frac{3p-1}{2(p+1)}(\Delta t)\mathbf{a}_i - \frac{p-3}{2(p+1)}(\Delta t)\mathbf{a}_{i+1}
\end{aligned} \tag{17}$$

where $\mathbf{M}$, $\mathbf{C}_0$ and $\mathbf{K}$ are the mass, viscous damping and stiffness matrices; $\mathbf{d}_i$, $\mathbf{v}_i$, $\mathbf{a}_i$ and $\mathbf{f}_i$ are nodal vectors of displacement, velocity, acceleration and external force, respectively; and the coefficient matrices of $\mathbf{B}_0$ to $\mathbf{B}_3$ are found to be

$$\mathbf{B}_0 = -\mathbf{D}^{-1}\frac{p-1}{8}\left(\frac{2}{p+1}\right)^3(\Delta t)^2\mathbf{K}_0 \qquad \mathbf{B}_1 = \mathbf{I} + \mathbf{D}^{-1}\frac{p-1}{8}\left(\frac{2}{p+1}\right)^3(\Delta t)^2\mathbf{K}_0$$

$$\mathbf{B}_2 = \mathbf{D}^{-1}\left[\mathbf{M} - \frac{p-3}{2(p+1)}(\Delta t)\mathbf{C}_0\right] \qquad \mathbf{B}_3 = \mathbf{D}^{-1}\left\{\tfrac{1}{2}\mathbf{M} - \tfrac{1}{4}\left[\left(\frac{2}{p+1}\right)^2 + \frac{p-3}{p+1}\right](\Delta t)\mathbf{C}_0\right\} \quad (18)$$

$$\mathbf{D} = \mathbf{M} - \frac{p-3}{2(p+1)}(\Delta t)\mathbf{C}_0 + \frac{p}{4}\left(\frac{2}{p+1}\right)^3(\Delta t)^2\mathbf{K}_0$$

where $\mathbf{K}_0$ is introduced to represent the initial stiffness matrix and the stiffness matrix $\mathbf{K}$ in the first line of Eq. (17) is generally different from the initial tangent stiffness $\mathbf{K}_0$ for a nonlinear system.

It is important to note that the coefficients matrices $\mathbf{B}_0$ to $\mathbf{B}_3$ must be determined by using the initial structural properties of $\mathbf{M}$, $\mathbf{C}_0$ and $\mathbf{K}_0$ as well as the step size before performing the time integration. The second line of Eq. (17) reveals that PFM is a two-step method. Hence, it seems that a different starting procedure is needed. However, the term $\mathbf{B}_0\mathbf{d}_{i-1}$ in the second line of Eq. (17) will disappear if $p=1$ is adopted. This implies that the starting procedure can be simply achieved by using $p=1$ to complete the computation of the first time step. Subsequently, any appropriate p value can be chosen to conduct the whole step-by-step integration procedure. The computation details for the $(i+1)-th$ time step is described next after computing the $i-th$ time step. At first, the displacement vector $\mathbf{d}_{i+1}$ can be directly calculated by using the second line of Eq. (17) without any nonlinear iterations since the coefficients matrices $\mathbf{B}_0$ to $\mathbf{B}_3$ are already know. In general, its computing procedure can be alternatively transformed into solving the following equation:

$$\left[\mathbf{M} - \frac{p-3}{2(p+1)}(\Delta t)\mathbf{C}_0 + \frac{p}{4}\left(\frac{2}{p+1}\right)^3(\Delta t)^2\mathbf{K}_0\right]\mathbf{d}_{i+1} = \frac{p-1}{8}\left(\frac{2}{p+1}\right)^3(\Delta t)^2\mathbf{K}_0(\mathbf{d}_i - \mathbf{d}_{i-1})$$

$$+\left[\mathbf{M} + \frac{p}{4}\left(\frac{2}{p+1}\right)^3(\Delta t)^2\mathbf{K}_0\right]\mathbf{d}_i + \left[\mathbf{M} - \frac{p-3}{2(p+1)}(\Delta t)\mathbf{C}_0\right](\Delta t)\mathbf{v}_i \quad (19)$$

$$+\left\{\tfrac{1}{2}\mathbf{M} - \tfrac{1}{4}\left[\left(\frac{2}{p+1}\right)^2 + \frac{p-3}{p+1}\right](\Delta t)\mathbf{C}_0\right\}(\Delta t)^2\mathbf{a}_i$$

In general, Eq. (19) consists of a set of equations and must be solved to obtain the next step displacement vector. This equation is often solved by a direction elimination method, which is usually made up of a triangulation and a substitution. It should be mentioned that the triangulation is required to be conducted only once since it is invariant for a complete step-by-step integration procedure. It is recognized that a triangulation will consume much more computational efforts than a substitution in a direct elimination method. Since the triangulation is needed to be performed only once in the solution of a nonlinear system for a complete step-by-step integration procedure, thus PFM will involve commensurate computational efforts per time step when compared to an explicit method, such as the well-known Newmark explicit method. In fact, the additional computational efforts are to perform the triangulation of the matrix in the left hand side of Eq. (19).

After obtaining the current displacement vector, the assumed fore-displacement relations can be applied to determine the corresponding restoring force vector. In general, $\mathbf{R}_{i+1} = \mathbf{K}\mathbf{d}_{i+1}$ is often used to represent the restoring force vector. Next, the velocity vector can be further evaluated from the substitution of the first line into the third line of Eq. (17) and is found to be

$$\mathbf{v}_{i+1} = \left[\mathbf{M} - \frac{p-3}{2(p+1)}(\Delta t)\mathbf{C}_0\right]^{-1} \left\{\mathbf{M}\left[\mathbf{v}_i + \frac{3p-1}{2(p+1)}(\Delta t)\mathbf{a}_i\right] - \frac{p-3}{2(p+1)}(\Delta t)\left[\frac{2p}{p+1}\mathbf{f}_{i+1} - \frac{p-1}{p+1}\mathbf{f}_i - \frac{2p}{p+1}\mathbf{R}_{i+1} - \frac{p-1}{p+1}\mathbf{R}_i\right]\right\} \tag{20}$$

Finally, the acceleration vector can be calculated by using the equations of motion, i.e., the first line of Eq. (17).

7. Numerical examples

Some numerical examples are examined in this section to confirm the numerical properties of PFM for both linear elastic and nonlinear systems. In these numerical investigations, the numerical properties of accuracy, unconditional stability and numerical dissipation are addressed. In addition, the computational efficiency of PFM is also explored in contrast to NEM and AAM. For brevity, PFM1 and PFM2 are introduced to represent the use of PFM with $p = 1$ and 0.5, respectively.

7.1 Example 1 --- An elastoplastic system

A single degree of freedom system subject to an earthquake record is considered. The lumped mass and the stiffness for the system are taken to be 10^4kg and 10^6N/m, respectively. Thus, the initial natural frequency of the system is found to be 10rad/sec before it deforms into an inelastic range. An elastoplastic behavior is assumed for the system during vibration. In addition, the yielding strength is assumed to be $5 \times 10^4 \text{N}$ for both tension and compression. The undamped system is excited by the ground acceleration record of CHY028 with a peak ground acceleration of

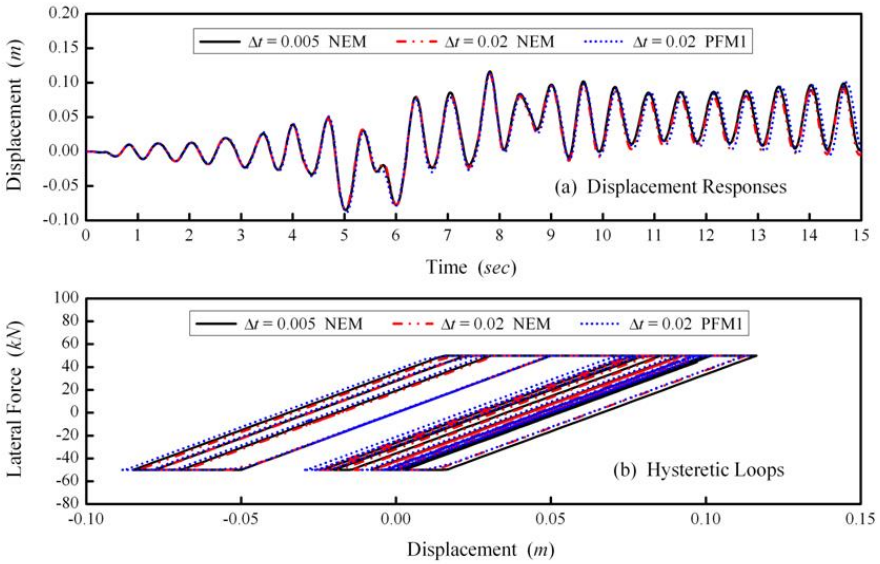

Fig. 6 Responses to CHY028 and corresponding hysteretic loops

0.5g. It should be mentioned that CHY028 is a near-fault ground motion record collected by the Central Weather Bureau under the Taiwan Strong Motion Instrumentation Program during the main shock of Chi-Chi earthquake.

Fig. 6 shows the displacement response time histories and their corresponding hysteretic loops. Numerical solutions obtained from NEM with a time step of $\Delta t = 0.005$ sec are considered as reference solutions for comparisons. Both NEM and PFM1 with the time step of $\Delta t = 0.02$ sec, which corresponds to $\Delta t / T_0 = 0.03$, are used to perform the step-by-step integration. In Fig. 6a, the displacement responses obtained from NEM and PFM1 are very close to the reference solutions. A slight difference between the results obtained from NEM and PFM1 and the reference solutions might be due to the fact that the yielding point is not exactly captured. Fig. 6b reveals that the system experiences highly nonlinear hysteretic behaviors. Thus, it is confirmed that PFM1 can be used to solve a highly nonlinear system.

7.2 Example 2 --- Free vibration responses of 5-story building

Fig. 7 shows an idealized 5-story shear building and its structural properties. Although the mass is distributed throughout the building, it is idealized as concentrated at the floor levels. The beams and floor systems are assumed to be rigid in flexure and the axial deformation of the beams and columns are neglected. The stiffness of each story consists of a linear part and a nonlinear part. The linear part is a constant stiffness and the nonlinear part is assumed to be a function of the story drift. The explicit expression of the stiffness for each story can be written in the form of

$$k_{j-i} = k_{0-i}\left[1 + p_i\left(\left|u_i - u_{i-1}\right|\right)^{1/5}\right] \quad , \quad i = 1 \sim 5 \tag{21}$$

where k_{j-i} is the instantaneous stiffness for the $i-th$ story at the end of the $j-th$ time step and k_{0-i} is the initial stiffness for the $i-th$ story at the start of the motion; $|u_i - u_{i-1}|$ is the story drift for the $i-th$ story and p_i is a given constant corresponding to this story drift. The initial natural frequencies and the 1st, 4th and 5th modal shapes of the building are also shown in Fig. 7. As a result, the equation of motion can be expressed as:

$$\begin{bmatrix} m_1 & 0 & 0 & 0 & 0 \\ 0 & m_2 & 0 & 0 & 0 \\ 0 & 0 & m_3 & 0 & 0 \\ 0 & 0 & 0 & m_4 & 0 \\ 0 & 0 & 0 & 0 & m_5 \end{bmatrix} \begin{Bmatrix} \ddot{u}_1 \\ \ddot{u}_2 \\ \ddot{u}_3 \\ \ddot{u}_4 \\ \ddot{u}_5 \end{Bmatrix} + \begin{bmatrix} k_{j-1}+k_{j-2} & -k_{j-2} & 0 & 0 & 0 \\ -k_{j-2} & k_{j-2}+k_{j-3} & -k_{j-3} & 0 & 0 \\ 0 & -k_{j-3} & k_{j-3}+k_{j-4} & -k_{j-4} & 0 \\ 0 & 0 & -k_{j-4} & k_{j-4}+k_{j-5} & -k_{j-5} \\ 0 & 0 & 0 & -k_{j-5} & k_{j-5} \end{bmatrix} \begin{Bmatrix} u_1 \\ u_2 \\ u_3 \\ u_4 \\ u_5 \end{Bmatrix} = \begin{Bmatrix} 0 \\ 0 \\ 0 \\ 0 \\ 0 \end{Bmatrix} \quad (22)$$

where the values of m_1 to m_5 are given in Fig. 7 and k_{j-1} to k_{j-5} are defined in Eq. (21) with the specified values of k_{0-1} to k_{0-5} in Fig. 7. A linear elastic system and a nonlinear system are simulated by specifying appropriate p_i values, which are given as below:

$$\begin{array}{lll} \text{LS} & p_1 \sim p_5 = 0.0 & \text{a linear elastic system} \\ \text{NS} & p_1 = -1.0, \quad p_2 \sim p_5 = -0.5 & \text{a linear elastic system} \end{array} \quad (23)$$

To confirm the effectiveness of the numerical dissipation, two initial conditions are considered. One is made up of the pure first mode only, i.e., $\mathbf{v}_1(0) = \phi_1 / 10$, and the other consists of the 1st, 4th and 5th modes with equal weight, i.e., $\mathbf{v}_2(0) = (\phi_1 + \phi_4 + \phi_5)/10$. The free vibration response to $\mathbf{v}_1(0)$ is obtained from NEM with the time step of $\Delta t = 0.0002$ sec. Meanwhile, the free vibration responses to $\mathbf{v}_2(0)$ are computed by AAM, PFM1 and PFM2 with a time step of $\Delta t = 0.01$ sec for LS and NS.

Numerical results are plotted in Figs. 8 and 9 for LS and NS, respectively. In each figure, the top plot displays the displacement response for the 1st story while that for the 5th story is plotted in

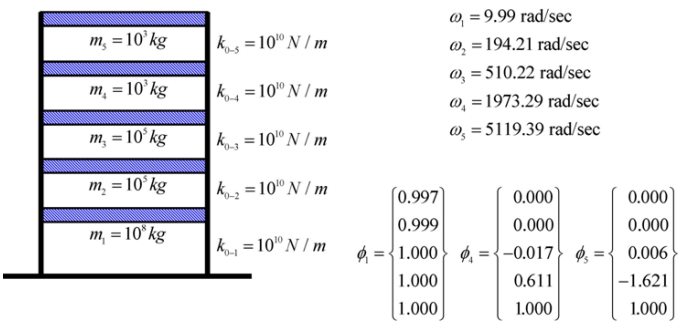

Fig. 7 A 5-story shear-beam type building

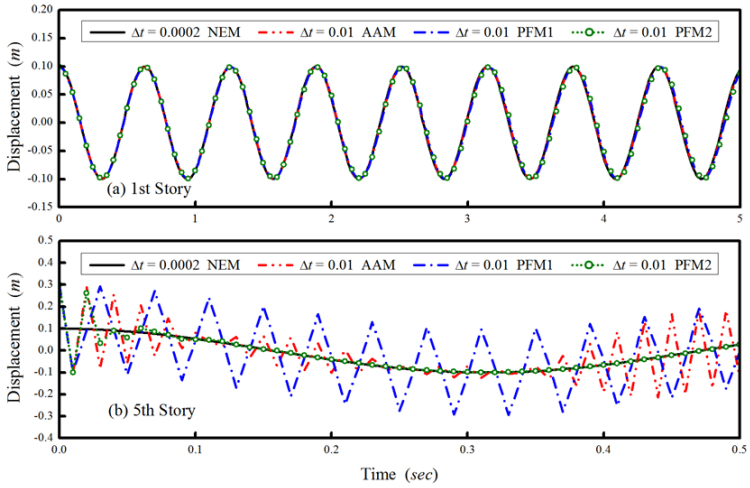

Fig. 8 Free vibration responses of LS

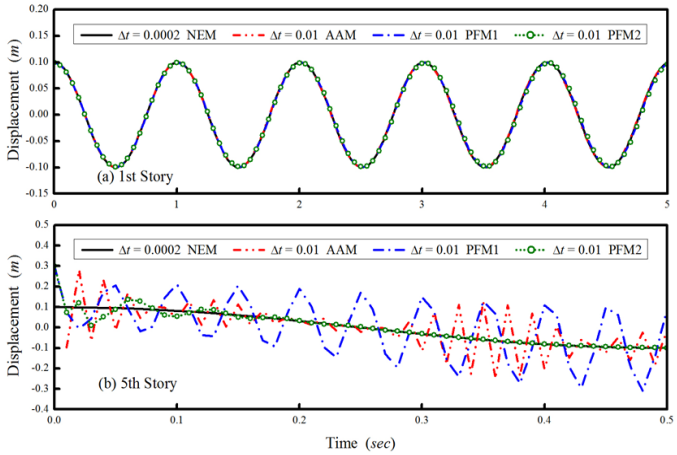

Fig. 9 Free vibration responses of NS

Table 1 Numerical damping ratio for each mode if using PFM2

System	$\overline{\xi}_{i+1}$ (1st mode)	$\overline{\xi}_{i+1}$ (2nd mode)	$\overline{\xi}_{i+1}$ (3rd mode)	$\overline{\xi}_{i+1}$ (4th mode)	$\overline{\xi}_{i+1}$ (5th mode)
LS	0.00%	4.21%	11.14%	17.65%	19.77%
NS	0.00%	4.90%	13.41%	21.00%	23.77%

the bottom plot. Only the first $0.5\,\text{sec}$ displacement response time history is plotted in the bottom plot of each figure so that the effectiveness of numerical damping to suppress the 4th and 5th modal responses can be closely examined. It is manifested from Figs. 8a and 9a that the four curves are coincided together. This is because that the contribution from the 4th and 5th modes to the total response at the 1st story is insignificant; and the time step of $\Delta t = 0.01\,\text{sec}$ is small enough for

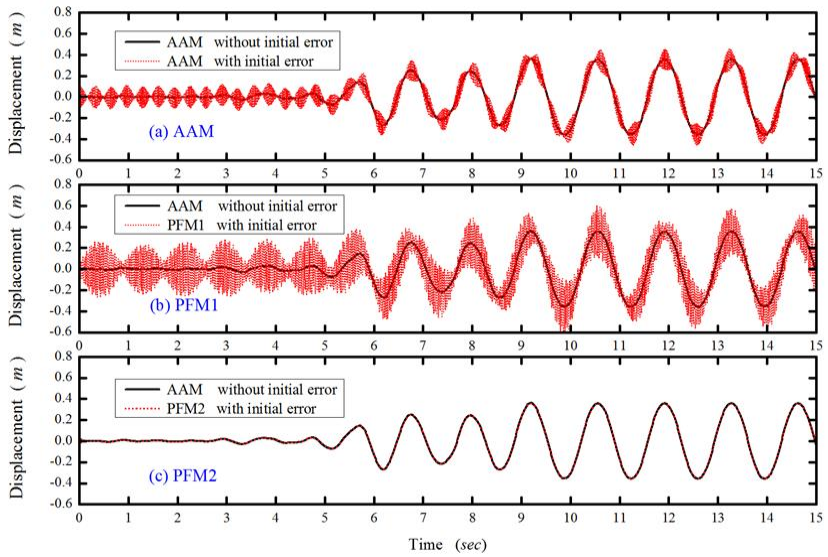

Fig. 10 Elimination of high frequency responses for NS subject to earthquake record CHY028

AAM, PFM1 and PFM2 to accurately integrate the 1st mode. Figs. 8b and 9b reveal that the contribution from the 4th and 5th modes to the total response at the 5th story is much more significant that for the 1st mode. In addition, it is also seen that both AAM and PFM1 cannot remove the 4th and 5th modal responses while they are eliminated very rapidly if using PFM2. In fact, PFM2 can filter out the high frequency responses within about $0.1\,\text{sec}$ for both LS and NS. This is because it can provide very large numerical damping ratios for the 4th and 5th modes as shown in Table 1. The details for obtaining the numerical damping ratio for each mode for a nonlinear system for each time step can be found in the references (Chang 2009, 2010) and will not elaborated here again. Since the numerical damping ratio varies with the stiffness change for a nonlinear system, the value for NS is an average value while it is constant for LS. Comparing Figs. 9 to 8, it is apparent that the period for NS is elongated for the 1st mode in contrast to that of LS. Thus, NS is experienced stiffness softening.

It is numerically illustrated that PFM can have favorable numerical dissipation. In fact, there is no numerical dissipation for PFM1 ($p=1$) while PFM2 ($p=0.5$) has desired numerical damping to suppress or eliminate the high frequency responses. The unconditional stability of PFM is also strongly indicated in step-by-step solution of both LS and NS since the product of the highest initial natural frequency and the step size is as large as 51.19 in this example.

7.3 Example 3 --- Seismic responses of 5-story building

In this example, the 5-story building with the p_i values defined in Eq. (23) for NS is also considered here. The building is also subjected to the earthquake record of CHY028 with a peak ground acceleration of 0.5g. In addition, the spurious oscillations due to the 5th mode are assumed at the beginning of the motion. As a result, an initial displacement vector of $\mathbf{v}(0)=\phi_5/10$ is

added in addition to the earthquake load. The top story responses are plotted in Fig. 10. The result obtained from AAM only subject to CHY028 is considered as a reference solution. On the other hand, AAM, PFM1 and PFM2 are also used to calculate the responses to both the earthquake load CHY028 and the initial displacement vector $\mathbf{v}(0) = \phi_5 / 10$. All the computations are carried out by using a time step of $\Delta t = 0.01\,\text{sec}$.

Numerical results for the top story responses are plotted in Fig. 10. It is clear that the results obtained from AAM and PFM1 are severely contaminated or even destroyed by the high frequency initial displacement vector while that obtained from PFM2 is almost coincided with the reference solution. This is because that PFM2 can have desired numerical dissipation to filter out the high frequency response while both AAM and PFM1 do not have any numerical dissipation. It is also interesting to find that the response obtained from AAM is less contaminated when compared to PFM1.

7.4 Example 4 --- A fixed-fixed beam

A fixed-fixed beam is loaded by a sinusoidal function at the center of the beam. The dimension and structural properties of the beam are the density of $\rho = 7.8\times10^{-6}\ kg/mm^3$, Young's modulus of $E = 2.0\times10^5\ N/mm^2$, sectional modulus of $I = 7.2\times10^3\ mm^4$, sectional area of $A = 6.0\times10^2\ \ mm^2$ and the length of $L = 4.5\times10^3\ mm$. The beam was modelled by 10 beam elements where each node has only the vertical and rotational degrees of freedom, leading to a total of 18 degrees of freedom. A consistent mass matrix is used in the analysis and the material is taken as linearly elastic. For a nonlinear analysis, both the elastic stiffness matrix and geometric stiffness matrix are used in the formulation of the structural stiffness matrix. Hence, the natural frequencies of the beam vary due to the geometric nonlinearity. The natural frequencies of the first three modes are found to be 19.38, 53.44 and 104.83 rad/sec based on the elastic stiffness matrix only. The nonlinear system is subjected to the sinusoidal force of $1.0\times10^5 \sin(2\pi t)\ \ N$ at

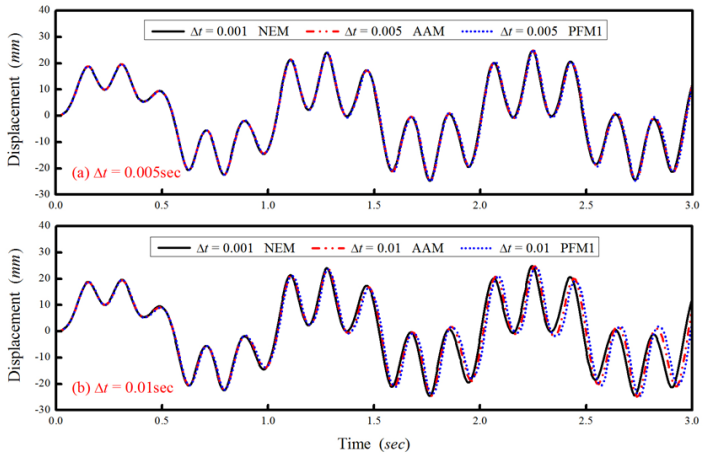

Fig. 11 Displacement responses at the center of a fixed-fixed beam

the center of the beam. Numerical results are plotted in Fig. 11. The numerical solution obtained from NEM with $\Delta t = 0.001\,\text{sec}$ is a reference solution. Meanwhile, AAM and PFM1 are also used to compute the responses by using the time steps of $\Delta t = 0.005$ and $0.01\,\text{sec}$. Fig. 11a reveals that both AAM and PFM1 with $\Delta t = 0.005\,\text{sec}$ can provide pretty reliable solutions. Whereas, both methods exhibit visible period distortion for using $\Delta t = 0.01\,\text{sec}$. It is also found that PFM1 shows a little more period distortion than for AAM. In general, PFM1 has comparable accuracy when compared to AAM, which is an energy conserving method (Simo *et al*. 1992; Gonzalez and Simo 1996).

7.5 Example 5 --- Computational efficiency

A large spring-mass system is considered for the study of the computational efficiency of PFM. This spring-mass system and its structural properties are shown in Fig. 12. The stiffness k_i of each spring will decrease after the system deforms due to the nonlinear term of $-10^9\sqrt{|u_i - u_{i-1}|}$. It is clear that the total number of the spring-mass system can be arbitrarily specified. Thus, in order to simulate a 500-DOF system and a 1000-DOF system, the cases of $n = 500$ and 1000 are taken. It is found that the lowest natural frequency of the 500-DOF system is $31.38\,\text{rad/sec}$ before it deforms while that for 1000-DOF system is $15.70\,\text{rad/sec}$. On the other hand, the two systems have the same highest natural frequency and are found to be $20000.0\,\text{rad/sec}$. In this study, NEM, AAM and PFM2 are used to calculate the displacement responses. Both spring-mass systems are excited by the combinations of sine loads as shown in Fig. 12.

Fig. 13 shows the displacement response time histories of the two systems. Since the highest natural frequency is as large as $20000.0\,\text{rad/sec}$ for both systems a time step must be chosen to be less than or equal to $\Delta t = 0.0001\,\text{sec}$ to satisfy the stability conditions for NEM. As a result, the numerical solutions obtained from this time step can be considered as "**exact**" solutions since this time step is much smaller than that required by accuracy consideration. Meanwhile, a comparable accuracy can be found for the numerical results obtained from AAM and PFM2 with a time step of $\Delta t = 0.005\,\text{sec}$ for the two systems. In addition, numerical experiments reveal that this time step seems to be the maximum time step to yield reliable solutions for both AAM and PFM2 in the solution of the 500-DOF and 1000-DOF systems. In general, it is computationally inefficient to use a conditionally stable method to solve an inertial problem, where the total response is dominated by low frequency modes and high frequency modes contribute insignificantly. In this example, the use of NEM is proposed to illustrate the importance of the unconditional stability for PFM2 since both NEM and PFM2 can have the explicitness for each time step.

In order to evaluate the computational efficiency of PFM, the CPU time involved for each analysis is recorded and summarized in Table 1 for NEM, AAM and PFM2. The CPU time consumed by NEM is denoted by $\text{CPU}^{(\text{NEM})}$. Similarly, $\text{CPU}^{(\text{AAM})}$ and $\text{CPU}^{(\text{PFM2})}$ are used to represent the CPU time consumed by AAM and PFM2. The fourth column of Table 1 reveals that PFM2 involves much less computational efforts when compared to both NEM and AAM. This is also manifested from the fifth and sixth columns. Clearly, NEM is computationally inefficient to solve the inertial problems since it costs a large CPU time for each analysis. This is because that a very small time step, which is much small than accuracy consideration, is generally needed so that the upper stability limit can be satisfied. On the other hand, although a relatively large time step

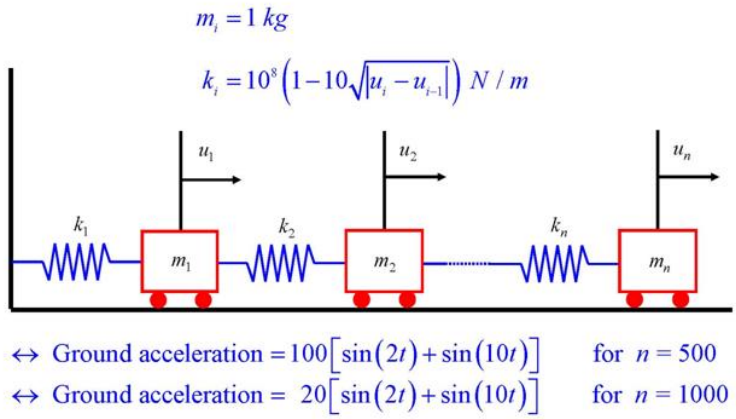

Fig. 12 A n-degree-of-freedom spring-mass system

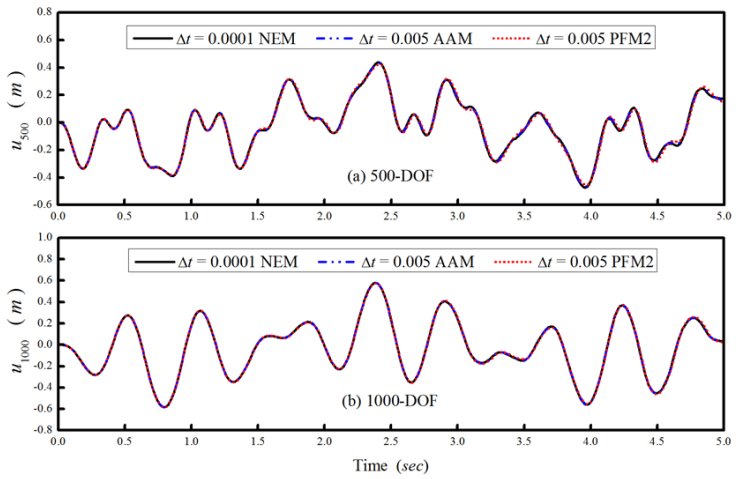

Fig. 13 Displacement responses to spring-mass systems

Table 2 Comparison of CPU time

N-DOF	$CPU^{(NEM)}$	$CPU^{(AAM)}$	$CPU^{(PFM2)}$	$\frac{CPU^{(PFM2)}}{CPU^{(NEM)}}$	$\frac{CPU^{(PFM2)}}{CPU^{(AAM)}}$
500	640.69	1733.47	32.94	0.051	0.019
1000	2955.91	14224.70	140.81	0.048	0.0099

can be applied for AAM based on accuracy consideration due to its unconditional stability, it still consumes many computational efforts as shown in the third column. This is because that an iteration procedure is needed in each time step for an implicit method and it is very time

consuming for a matrix of large order. Since PFM2 can integrate the unconditional stability and the explicitness of each time step, which involves no nonlinear iterations for each time step, it can save many computational efforts.

8. Conclusions

In this paper, a parameter p is applied to develop a new family of integration methods for structural dynamics. In general, numerical properties of the proposed family method are controlled by the parameter p. An appropriate selection of $1/2 \le p \le 1$ will lead to unconditional stability and favorable numerical dissipation, which can be continuously controlled by p and it is possible to achieve zero numerical damping if $p = 1$ is adopted. This numerical damping can be used to suppress or even eliminate the spurious participation of high frequency modes while the low frequency modes can be accurately integrated. Comparing to the currently available dissipative integration methods, the most important improvement of this family method is that it involves no nonlinear iterations for each time step in addition to unconditional stability and desired numerical dissipation. As a result, it is computationally very efficient for solving an inertial-type problem.

Acknowledgement

The author is grateful to acknowledge that this study is financially supported by the National Science Council, Taiwan, R.O.C., under Grant No. NSC-99-2221-E-027-029.

References

Bathe, K.J. (1986), *Finite Element Procedure in Engineering Analysis*, Prentice-Hall, Inc., Englewood Cliffs, N.J., USA.

Bathe, K.J. and Wilson, E.L. (1973), "Stability and accuracy analysis of direct integration methods", *Earthq. Eng. Struct. Dyn.*, **1**(3), 283-291.

Belytschko, T. and Schoeberle, D.F. (1975), "On the unconditional stability of an implicit algorithm for nonlinear structural dynamics", *J. Appl. Mech.*, **42**(4), 865-869.

Belytschko, T. and Hughes, T.J.R. (1983), *Computational Methods for Transient Analysis*, Elsevier Science Publishers B.V., North-Holland.

Chang, S.Y. (1997), "Improved numerical dissipation for explicit methods in pseudodynamic tests", *Earthq. Eng. Struct. Dyn*, **26**(9), 917-929.

Chang, S.Y. (2000), "The γ-function pseudodynamic algorithm", *J. Earthq. Eng.*, **4**(3), 303-320.

Chang, S.Y. (2002), "Explicit pseudodynamic algorithm with unconditional stability", *J. Eng. Mech.*, ASCE, **128**(9), 935-947.

Chang, S.Y. (2007), "Improved explicit method for structural dynamics", *J. Eng. Mech.*, ASCE, **133**(7), 748-760.

Chang, S.Y. (2009), "An explicit method with improved stability property", *Int. J. Numer. Method Eng.*, **77**(8), 1100-1120.

Chang, S.Y. (2010), "A new family of explicit method for linear structural dynamics", *Comput. Struct.*, **88**(11-12), 755-772.

Chung, J. and Hulbert, G.M. (1993), "A time integration algorithm for structural dynamics with improved numerical dissipation: the generalized-α method", *J. Appl. Mech.*, **60**(6), 371-375.
Dobbs, M.W. (1974), "Comments on 'stability and accuracy analysis of direct integration methods by Bathe and Wilson", *Earthq. Eng. Struct. Dyn.*, **2**, 295-299.
Goudreau, G.L. and Taylor, R.L. (1972), "Evaluation of numerical integration methods in elasto-dynamics", *Comput. Method. Appl. Mech. Eng.*, **2**(1), 69-97.
Hilber, H.M., Hughes, T.J.R. and Taylor, R.L. (1977), "Improved numerical dissipation for time integration algorithms in structural dynamics", *Earthq. Eng. Struct.Dyn.*, **5**(3), 283-292.
Hilber, H.M. and Hughes, T.J.R. (1978), "Collocation, dissipation, and 'overshoot' for time integration schemes in structural dynamics", *Earthq. Eng. Struct. Dyn.*, **6**(1), 99-118.
Hughes, T.J.R. (1987), *The Finite Element Method*, Prentice-Hall, Inc., Englewood Cliffs, NJ, USA.
Krieg, R.D. (1973), "Unconditional stability in numerical time integration methods", *J. Appl. Mech.*, **40**(2), 417-421.
Lambert, J.D. (1973), *Computational Methods in Ordinary Differential Equations*, John Wiley, London, UK.
Lax, P.D. and Richmyer, R.D. (1956), "Survey of the stability of linear difference equations", *Commun. Pure Appl. Math.*, **9**(2), 267-293.
Newmark, N.M. (1959), "A method of computation for structural dynamics", *J. Eng. Mech. Div., ASCE*, **85**(3), 67-94.
Simo, J.C., Tarnow, N. and Wong, K.K. (1992), "Exact energy-momentum conserving algorithms and symplectic schemes for nonlinear dynamics", *Comput. Method. Appl. Mech. Eng.*, **100**(1), 63-116.
Gonzalez, O. and Simo, J.C. (1996), "On the stability of symplectic and energy-momentum algorithms for non-linear Hamiltonian systems with symmetry", *Comput. Method. Appl. Mech. Eng.*, **134**(3-4), 197-222.
Wood, W.L., Bossak, M. and Zienkiewicz, O.C. (1981), "An alpha modification of Newmark's method", *Int. J. Numer. Method. Eng.*, **15**(10), 1562-1566.
Zhou, X. and Tamma, K.K. (2004), "Design, analysis and synthesis of generalized single step single solve and optimal algorithms for structural dynamics", *Int. J. Numer. Method. Eng.*, **59**(5), 597-668.
Zhou, X. and Tamma, K.K. (2006), "Algorithms by design with illustrations to solid and structural mechanics/ dynamics", *Int. J. Numer. Method. Eng.*, **66**(11), 1841-1870.
Zienkiewicz, O.C. (1977), *The Finite Element Method*, (3rd Edition), McGraw-Hill Book Co. Ltd., UK.

IT